Black carbon content of traffic emissions impacts significantly on black carbon mass size distributions and mixing states

Fei Li[1,3,5#], Biao Luo [2,4#], Miaomiao Zhai[2,4], Li Liu[3], Gang Zhao[7], Hanbing Xu[6], Tao Deng[3], Xuejiao Deng[3], Haobo Tan[3], Ye Kuang[2,4*], Jun Zhao[1*]

[1] School of Atmospheric Sciences, Guangdong Province Key Laboratory for Climate Change and Natural Disaster Studies, and Southern Marine Science and Engineering Guangdong Laboratory (Zhuhai), Sun Yat-sen University, Zhuhai, 519082, China

[2] Institute for Environmental and Climate Research, Jinan University, Guangzhou, 511443, China.

[3] Institute of Tropical and Marine Meteorology, China Meteorological Administration, Guangzhou, 510640,China

[4] Guangdong-Hongkong-Macau Joint Laboratory of Collaborative Innovation for Environmental Quality, Guangzhou, 511443, China.

[5] Xiamen Key Laboratory of Straits Meteorology, Xiamen Meteorological Bureau, Xiamen, 361012, China

[6] Experimental Teaching Center, Sun Yat-Sen University, Guangzhou 510275, China

[7] State Key Joint Laboratory of Environmental Simulation and Pollution Control, International Joint Laboratory for Regional Pollution Control, Ministry of Education, College of Environmental Sciences and Engineering, Peking University, Beijing, 100871, China

# These authors contribute equally to this paper.

Corresponding author: Ye Kuang (kuangye@jnu.edu.cn) and Jun Zhao

(zhaojun23@mail.sysu.edu.cn)

Abstract

Both the size and mixing state of black carbon (BC)-containing aerosols are crucial in estimating the environmental, health and climate impacts of BC. Traffic emissions are a major global source of BC, however, parameterization of BC mass size distributions and mixing states associated with traffic remains lacking due to its dependence on vehicle types and driving conditions. To investigate BC mass size distributions and mixing states associated with traffic emissions, a field campaign was conducted in Guangzhou urban area during winter, which used a system coupling a differential mobility analyzer (DMA) and single-particle soot photometer (SP2) to measure BC mass size distributions in the range of 100 to 700 nm. The resolved primary organic aerosols were hydrocarbon-like organic aerosols (HOA) and cooking-like organic aerosols (COA), refractory BC (rBC) which was detected by the DMA-SP2 and correlated highly with HOA (R^2=0.88), confirming that traffic emissions are the dominant source of atmospheric BC during the observations. The BC mass size distribution was found to be best fitted by a lognormal distribution, with a geometric mean ($D_{g,BC}$) of 258±16 nm, varying between 200 and 300 nm. During daytime, active formation of secondary nitrate and organic aerosols was observed, but it had little effect on the variations of BC mass size distributions. Further analyses revealed that $D_{g,BC}$ was moderately correlated with rBC/HOA (R^2=0.41) in a linear form of $D_{g,BC}$= 34×rBC/HOA+177, demonstrating that the BC content of traffic emissions significantly impacts the BC mass size distributions. In addition, the size-dependent fractions of BC-containing aerosols in all types of aerosols (f_{BCc}) and the fraction of identified externally mixed (bare/thinly coated) BC particles in all BC-containing aerosols (f_{ext}) were also characterized. It was found that the daytime secondary aerosol formation reduced both f_{BCc} and f_{ext}, with the decrease of f_{ext} being more pronounced for larger particles, possibly due to the higher relative coating thickness. Variations in f_{ext} during nighttime were mainly controlled by the emission conditions. For example, f_{ext} for 600 nm particles decreased from 0.82 to 0.46 as rBC/HOA increased from 1 to 3.5 while the mass ratios of secondary aerosols to rBC varied little, demonstrating that the BC content also significantly affects the mixing states of freshly emitted BC from traffic emissions. This study suggests that BC content can be used as the key factor to parameterize both the BC mass size distribution and mixing states from traffic emissions, which warrants future comprehensive investigation. In addition, other sources such as biomass burning and coal combustion also contribute substantially to BC emissions, it was important to investigate whether

BC content of other major BC sources than traffic are also important in determining BC mass size distributions and mixing states. Overall, results of this study have significant implications for accurate representation of BC from different sources when modeling the impacts of BC.

1 Introduction

Aerosols impact significantly on human health through deposition on human tissues, visibility, weather and climate through interacting with solar radiation and acting as cloud condensation nuclei (CCN). Most of the atmospheric aerosols scatter readily while absorbing negligibly or little solar irradiation, but one exception is black carbon (BC) which absorbs solar irradiation strongly and thus heats the atmosphere. This strong absorption makes BC the second atmospheric warming component (Bond et al., 2013) and plays a major role in climate and air pollution (Zhang et al., 2019). Menon et al. (2002) found that BC's absorption could affect trends of droughts and floods in India and China by altering regional atmospheric stability and vertical motions. The heating effects of BC (Wang et al., 2013) in the atmospheric boundary layer can suppress boundary layer turbulence, impacting boundary layer development and meteorology (Wilcox et al., 2016), and consequently affecting local haze formation (Ding et al., 2016). Moreover, BC-containing aerosols can interact with clouds and serve as CCN (Zhang et al., 2017;Motos et al., 2019;Hu et al., 2021), thus indirectly impacting climate (Koch and Del Genio, 2010). These effects of BC can be quantitatively determined through its radiative forcing. In addition, inhalation of atmospheric BC also poses a threat to human health; evidence suggests that it may be associated with changes in subclinical cardiovascular health effects in individuals (Nichols et al., 2013).

The radiative and health effects of BC are highly dependent on its size and mixing state, as these factors determine the distribution of BC in aerosols and their optical properties (Bond et al., 2006), hygroscopic growth (Liu et al., 2013), and depositions in the human respiratory tract (Man et al., 2022). Detailed parameterizations of BC size and mixing states as well as aging of BC containing aerosols in models are crucial for modeling environmental and climate effects of BC (Wang et al., 2018). Freshly emitted BC can be either almost bare or coated with other materials, usually organic aerosols, which can then undergo rapid aging processes through vapor condensation or serving as medium for reactions (Zhang et al., 2018a;Zhang et al., 2020a;Zhang et al., 2021). This leads to size and morphological changes of BC-containing aerosols (Zhang et al., 2008) and influences their physical properties, such

as hygroscopicity (Liu et al., 2013) and activation abilities (Ding et al., 2019;Yu et al., 2022). The coating of other components on BC can also significantly affect the optical properties of BC-containing aerosols, such as the lensing effect that enhances light absorption (Bond et al., 2006;Peng et al., 2016). This effect is non-linear (Liu et al., 2017;Wang et al., 2021) and is highly dependent on the mixing state heterogeneity of BC-containing aerosols (Fierce et al., 2020;Zhao et al., 2021;Zhai et al., 2022a). In addition, Zhao et al. (2019) showed that the BC mass size distributions also play a major role in the direct radiative effects of BC. The size and mixing states of BC, as well as the chemical composition of its coatings, vary significantly with sources (Zhang et al., 2020b). This results in marked differences in the aging processes of freshly emitted BC from different sources in the atmosphere, depending on the emission sources and meteorological conditions in a given location.

Guangzhou is an expansive metropolis in the highly industrialized Pearl River Delta (PRD) region of China. Previous studies have shown that emissions from fossil fuel combustion are major sources of BC (Liu et al., 2014) while biomass burning emissions might also make certain contributions during autumn and winter (Sun et al., 2020). However, recent studies on source apportionment have not detected obvious signals attributed to biomass burning in autumn and winter, suggesting that other sources such as traffic activities are the main contributors to BC emissions (Guo et al., 2020;Chen et al., 2021b;Liu et al., 2022;Zhai et al., 2022b). Few studies have used the single-particle soot photometer (SP2) to measure bulk BC mass concentrations and mixing states in Guangzhou urban area (Huang et al., 2011; Tao et al., 2021). Furthermore, no comprehensive measurements that characterize both size distribution and mixing states of BC in this region have been conducted, and the factors that control variations in BC mass size distributions and mixing states remain unknown. BC emissions from diesel vehicles dominate traffic BC emissions (Bond et al., 2013) and depend on many factors, such as fuel type, engine operating conditions, engine types, driving patterns, and environmental conditions (Adler et al., 2010). These conditions have a significant impact on the size distributions and mixing states of emitted particles (Lähde et al., 2011;Xu et al., 2014), therefore BC mass size distributions and mixing states vary a lot in real traffic conditions. While numerous studies have examined the BC size and mixing states of emissions from various types of vehicles (Adler et al., 2010;Liu et al., 2017), only a few have directly investigated the BC size distribution and mixing states as a function of aerosol mobility diameter using the DMA-SP2 system which couples differential mobility analyzer (DMA) and SP2 (Raatikainen et al., 2017), and reported the average coating

characteristics of aerosol particles emitted from diesel vehicle exhaust (Han et al., 2019;Zhang et al., 2020b). However, the variations of BC mass size distributions and BC mixing states from real traffic emissions using the DMA-SP2 system have rarely been studied, and how to parameterize them remains elusive. This study carried out a field campaign and employed the DMA-SP2 system to investigate the dominant contribution of traffic emissions to atmospheric BC, which provided an ideal opportunity to evaluate how primary traffic emissions and their subsequent aging can affect BC mass size distributions and mixing states.

2 Materials and Methods

2.1 Campaign information

The campaign was conducted to characterize BC mass size distributions and mixing states from 11 January to 27 February 2022 at the Haizhu wetland park (23°05'N, 113°22'E) in Guangzhou. The instruments used for characterizing aerosol chemical and physical properties included a quadrupole aerosol chemical speciation monitor (Q-ACSM) for monitoring aerosol chemical compositions, a DMA-SP2 system for measuring BC mass size distributions and mixing states, and a scanning mobility particle sizer (SMPS) system for measuring aerosol particle number size distributions ranging from 13 nm to 800 nm. An AE33 aethalometer (Drinovec et al., 2015) was used to measure aerosol absorptions at multiple wavelengths and indirectly measure bulk BC mass concentrations. A $PM_{2.5}$ inlet (BGI, SCC 2.354) with a flow rate of 8 L/min was used for aerosol sampling. The flow rates of the Q-ACSM, CPC, SP2 and AE33 instruments were set to 3 L/min, 0.3 L/min, 0.1 L/min, and 5 L/min, respectively, to meet the flow rate requirement of the impactor although there are some deviations. All instruments were housed in a temperature-controlled container (23-27 ℃) and placed downstream of a Nafion drier designed to lower the sample RH to less than 35% (placed outside of the container and vertically to ensure a straight line of the sampling route so that sampling loss of aerosols can be minimized). Meteorological parameters such as temperature, wind speed and direction, and relative humidity (RH) were measured using an automatic weather station. Further details about this site can be found in Liu et al. (2022). In addition, concentrations of $PM_{2.5}$ and nitrogen dioxide (NO2) were obtained from China National Environmental Monitoring network which is publicly available (http://www.cnemc.cn/en/), there is a site located within 5 km distance to our observation site.

2.2 DMA-SP2 system and data processing

143   The SP2 (Droplet Measurement Technologies) can measure aerosol scattering and incandescence

144   signals of individual particles and identify if they contain detectable BC mass. It can also provide BC

145   mass concentrations at the single particle level, thus allowing for the determination of BC mixing states.

146   The scattering signals can be used to estimate the particle size of each BC-free particle; however, a

147   leading-edge-only method is required for sizing BC-containing particles (Schwarz et al., 2006), with

148   the estimated optical-equivalent size potentially deviating substantially from the mobility size due to

149   variations in aerosol refractive index and morphology. As such, the use of the DMA-SP2 system to

150   measure BC mass size distributions and mixing states has been previously proposed (Raatikainen et

151   al., 2017;Han et al., 2019;Sarangi et al., 2020;Zhao et al., 2021), which complement the size

152   measurements and additional size information can be used to derive physical properties such as

153   morphology and effective densities (Zhang et al., 2018b;Wu et al., 2019). A similar system has also

154   been used for other applications, such as investigation of the hygroscopic properties of BC-containing

155   aerosols (McMeeking et al., 2011; Liu et al., 2013). The DMA-SP2 set-up of Zhao et al. (2021)

156   employed a continuous scanning mode of the DMA, allowing for black carbon mass size distribution

157   (BCMSD) measurements with a time resolution of 5 minutes. However, accurate matching of the time

158   of particles in the DMA and SP2 is necessary. Some previous studies passed size-selected

159   monodisperse aerosols to the SP2 at only a few diameters (Zhang et al., 2018b;Han et al., 2019),

160   limiting the retrieval of BC mass size distributions and mixing states across the entire submicron

161   diameter range. In this study, we developed a software which enables the DMA to scan at different

162   diameters for different time periods depending on their number concentrations. For example, DMA

163   scans at 100 nm last about 36 seconds, while scans at 700 nm last about 1.5 minutes, allowing for

164   enough particles to be sampled at larger particle sizes. The diameter set points (18 points) of DMA

165   scans are 100 nm, 120 nm, 160 nm, 200 nm, 235 nm, 270 nm, 300 nm, 335 nm, 370 nm, 400 nm, 435

nm, 470 nm, 500 nm, 535 nm, 570 nm, 600 nm, 635 nm, and 700 nm, with a full scan taking 20 minutes.

With this set-up, the particle number size distributions of BC-containing and BC-free aerosols can be derived from the DMA-SP2 measurements using an inversion routine that mainly accounts for the effects of the DMA transfer function and multiple charge. Assuming a BC density of 1.8 g/cm^3, the BC volume equivalent diameter of each BC-containing particle (termed as BC core diameter, D_c) can be calculated, assuming a core-shell structure. The particle number size distribution of BC-containing aerosol, containing information of BC mixing states, can then be described using a two-variable formulation $\frac{\partial N}{\partial \log(Dp)\partial \log(Dc)}$, and the multiple charge correction method proposed by Zhao et
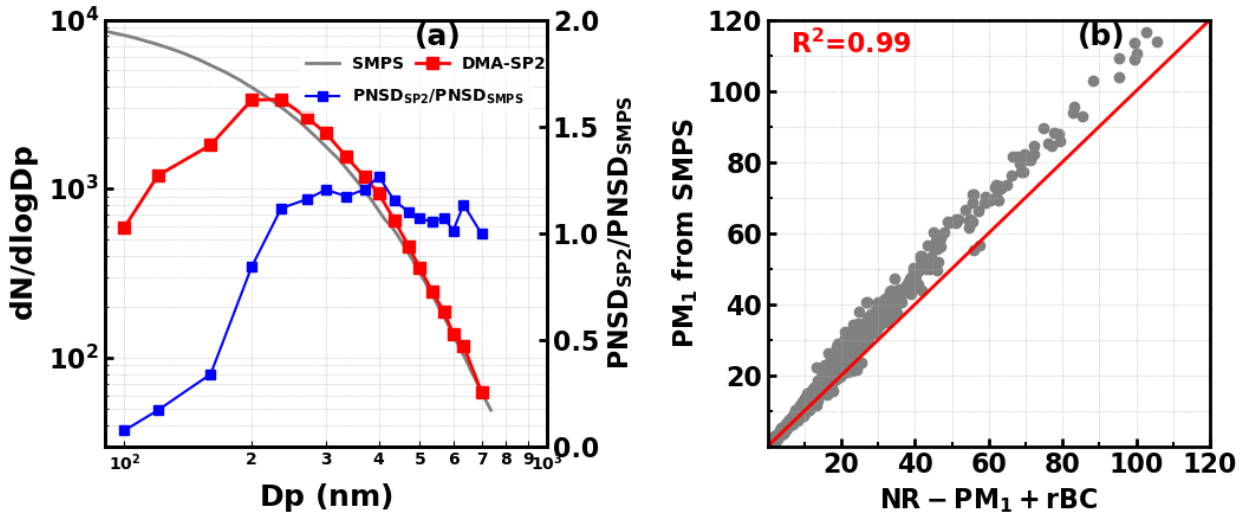
Figure 1. (a) Comparisons between average PNSD observed by the SMPS and inverted from the DMA-SP2 system; (b) Comparison between NR-PM$_1$+rBC and PM$_1$ mass concentrations calculated from SMPS measurements.

al. (2021) was used here to account for the impacts of multiple charge on $\frac{\partial N}{\partial \log(Dp)\partial \log(Dc)}$ derivations.

Using the derived $\frac{\partial N}{\partial \log(Dp)\partial \log(Dc)}$, the BC mass size distribution with multiple charge corrections accounted for can be derived through integrating rBC mass of each D_c. Details about the inversion routines are introduced in Sect. S1 of the supplement. Note that the effective density of bare BC or BC contained in a particle can vary substantially due to BC morphology and existence of air voids (Zhang et al., 2016;Zhao et al., 2020a). Therefore, a simple assumption of 1.8 g/cm^3 for BC density could bring uncertainties to D_c calculations. In addition, the optical equivalent diameter of BC-containing aerosols cannot be retrieved in this study due to the failure of the SP2 split channel hardware during the campaign, which rendered the leading-edge-only method unusable.

The average particle number size distribution (PNSD) derived from the DMA-SP2 system was compared with the one obtained from independent SMPS measurements, as shown in Fig. 1a. The detection limitations of the SP2 scattering channels (Raatikainen et al., 2017) caused the PNSD from SP2 to be markedly lower than that from SMPS for diameters <200 nm. For diameters larger than 200 nm, the PNSD from SP2 was generally consistent with that from SMPS, with the average ratio of SMPS to SP2 measurements being 0.89±0.05, which is similar to the phenomenon reported in Raatikainen et al. (2017), with an average ratio of 0.82. Additionally, the observed rBC mass concentrations correlated highly with the optically equivalent BC mass concentrations reported by the AE33 aethalometer (R^2=0.96, and an average ratio of 0.96), as shown in Fig. S4. The consistency tests between the DMA-SP2 system and SMPS measurements validated the number size distributions and BC mass concentrations inverted from DMA-SP2 measurements.

The number fractions of BC-containing aerosols of various diameters can be calculated using the DMA-SP2 measurements. Based on the time lag between the peak time of the scattering and the incandescence signal (Schwarz et al., 2006;Moteki and Kondo, 2007;Sedlacek Iii et al., 2012), these aerosols can be roughly divided into two categories: bare/thinly coated BC particles and thickly coated BC particles. The time lag distribution of pure BC aerosols can be identified from the SP2 calibrations using bare BC aerosols. Consequently, bare/thinly coated BC particles can be identified using the calibrated critical lag-time.

2.3 Q-ACSM measurements and positive matrix factorization (PMF) analysis

The Q-ACSM measured non-refractory sub-micrometer (NR-PM$_1$) species, including organic aerosol (OA), sulfate (SO$_4$), nitrate (NO$_3$), ammonium (NH$_4$), and chloride (Cl), at a time resolution of 15 minutes. More detailed description can be referred to Liu et al. (2022) and Ng et al. (2011). The mass spectra measured by the Q-ACSM were analyzed using ACSM standard data analysis software (ACSM Local 1.5.10.0 Released July 6, 2015), written in Igor Pro (version 6.37). The composition-dependent collection efficiency (CE) parameterization scheme proposed by Middlebrook et al. (2012) was used to calculate the mass concentrations of OA and inorganic species. This was also detailed in Liu et al. (2022). As calibration of the Q-ACSM was not available during this campaign, relative ionization efficiencies (RIEs) of 5.15 and 0.7 for ammonium and sulfate from previous calibrations were used, while the default RIEs of 1.4, 1.1, and 1.3 were used for organic aerosol, nitrate, and chloride, respectively. The quality assurance of the Q-ACSM measurements was first performed

through comparing the mass concentrations of PM_1 (summation of measured NR-PM_1 concentrations and rBC concentrations measured by the DMA-SP2 system) with PM_1 mass concentrations calculated from the particle number size distribution measurements of SMPS, assuming an aerosol density of 1.6 g/cm^3. Good consistency (as shown in Fig. 1b) was achieved between SMPS and Q-ACSM measurements (R^2=0.99), with NR-PM_1+rBC values slightly lower than PM_1 concentrations from SMPS (an average ratio of 1.19). Three reasons explain the deviations between SMPS and Q-ACSM plus rBC measurements: 1) the assumed average aerosol density may be biased from the real variations; 2) some aerosol species are not measured by the Q-ACSM, such as sub-micrometer dust; 3) Both Q-ACSM and SMPS have uncertainties with the aerosol mass spectrometer of about 30% (Ng et al., 2011;Fröhlich et al., 2013) and SMPS of different diameter ranges differ (Wiedensohler et al., 2012).

Following the same procedure of the PMF analysis for the Q-ACSM measurements introduced in Liu et al. (2022) and Zhai et al. (2022b), the PMF technique with the multilinear engine (ME-2) (Canonaco et al., 2013;Canonaco et al., 2021) was applied to ACSM spectra for deconvolving OA into different factors and detailed in the supplement. In total, four factors were identified, including two primary OA (POA) factors: a hydrocarbon-like OA (HOA, O/C~0.16) and a cooking-like OA (COA, O/C~0.14); and two oxygenated OA factors: a less oxidized oxygenated OA (LOOA, O/C~0.89) and a more oxidized oxygenated OA (MOOA, O/C~0.94). SOA was represented by the summation of LOOA and MOOA as done in previous studies (Kuang et al., 2020). The mass spectra of these factors, the determination of the factor number, the selection of solutions and more details about the factor analysis can be found in Sect. S2 of the supplement.

3 Results and discussion

3.1 Overview of aerosol chemical compositions

During the observation period, the $PM_{2.5}$ mass concentration varied significantly (from 1 to 126 $\mu g/m^3$) with an average of 20 $\mu g/m^3$ and several pollution episodes were observed during relatively stagnant conditions when wind speeds were near or below 1 m/s. The time series of meteorological parameters as well as $PM_{2.5}$, ammonium sulfate (AS), ammonium nitrate (AN), SOA, HOA, COA and rBC are shown in Fig. 2. The scheme proposed by Gysel et al. (2007) was used to identify AS and AN. On average, secondary aerosols including nitrate, sulfate, ammonium and SOA together accounted for

about 80% of non-refractory PM_1 mass concentration and secondary aerosols increased substantially during pollution episodes, demonstrating active secondary aerosol formations during the observations which might significantly impact BC mass size distributions as well as BC mixing states. The average air RH during the observations varied a lot from 42% to 98% with an average of 76%, suggesting that the heterogeneous reactions that involve aerosol water were favored during this campaign, which is consistent with the quick formation of ammonium nitrate in pollution episodes. On average, AN, AS and SOA accounted for 33%, 25% and 42% of secondary aerosols respectively, which is consistent with Zhai et al. (2022b) that nitrate concentrations are higher than sulfate during winter in Guangzhou urban area, especially under pollution conditions. The time series of rBC mass concentrations were shown in Fig. 2d, with rBC mass concentrations ranging from about 0.1 to 20 µg/m³ with an average of 2.3 µg/m³. Resolved POA factors were HOA and COA, which is consistent with results of previous studies in recent years that traffic emissions and cooking emissions are two main sources of primary aerosols in Guangzhou urban area (Guo et al., 2020;Chen et al., 2021a;Chen et al., 2021b). The rBC

correlated highly with HOA (R^2=0.88), demonstrating that traffic emissions contributed dominantly to
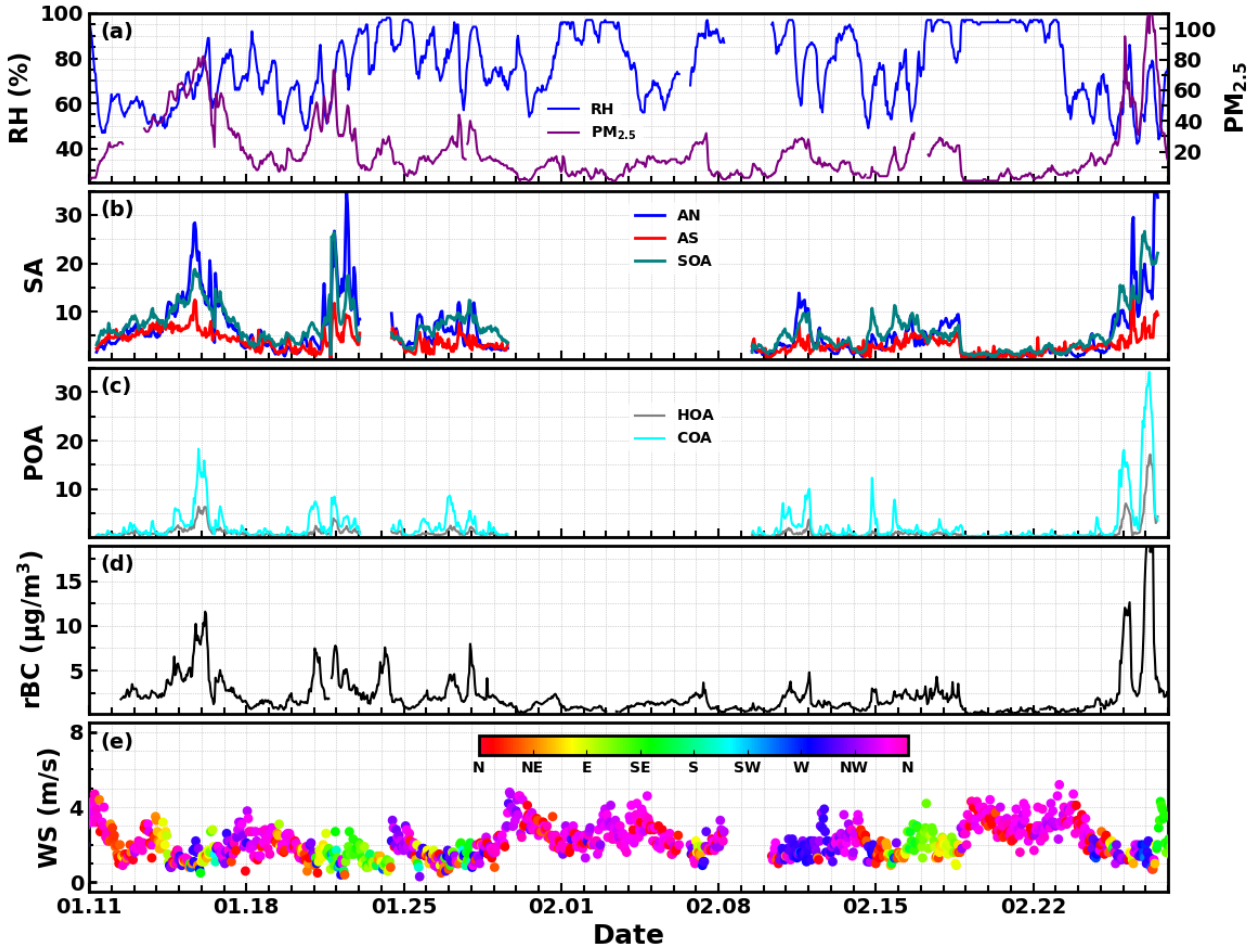
Figure 2. Timeseries of **(a)** RH and PM$_{2.5}$; **(b)** secondary aerosols including nitrate, sulfate and OOA; **(c)** HOA and COA; **(d)** rBC; **(e)** wind speed and directions.

atmospheric BC during the observations.

3.2 Overview of DMA-SP2 measurements

The observed average BC mass size distribution, as shown in Fig. 3a, exhibits a single lognormal mode for diameters greater than 100 nm, with a fitted geometric mean (D$_{g,BC}$) of 258 (±16) nm ranging from 200 nm to 300 nm. The formula form of fitting is introduced in Eq.1 of the supplement, and the mean of fitted geometric standard deviation (σ$_g$) is 1.69. A small mass mode might exist for diameters less than 100 nm; however, it cannot be characterized due to the detection limitation of the SP2, which measures BC-containing particles with a D$_c$ larger than 80 nm. Previous studies have reported BC mass size distribution as a function of rBC core diameter (Kompalli et al., 2020;Liu et al., 2019). The retrieved D$_{g,BC}$ is higher than most mass median diameters of rBC core measured in urban environments, near 200 nm in urban Beijing (Liu et al. (2019) which is reasonable due to intrinsic

267 coatings (Adler et al., 2010). Some prior studies reported BC mass size distribution as a function of

268 mobility diameter D_p measured by coupling the DMA with aethalometer (Stabile et al., 2012;Ning et

269 al., 2013;Zhao et al., 2019). A few studies also reported BC mass size distribution as a function of

270 aerodynamic diameter using the size-segregation filtering method (Hu et al., 2012). Zhao et al. (2019)

271 reported bimodal characteristics of BC mass size distribution in the North China Plain, with the second

272 mode accounting for most of the rBC mass and a $D_{g,BC}$ of the coarse mode ranging from 430 to 580

273 nm, which is much higher than the average one reported here. This difference may be attributed to the
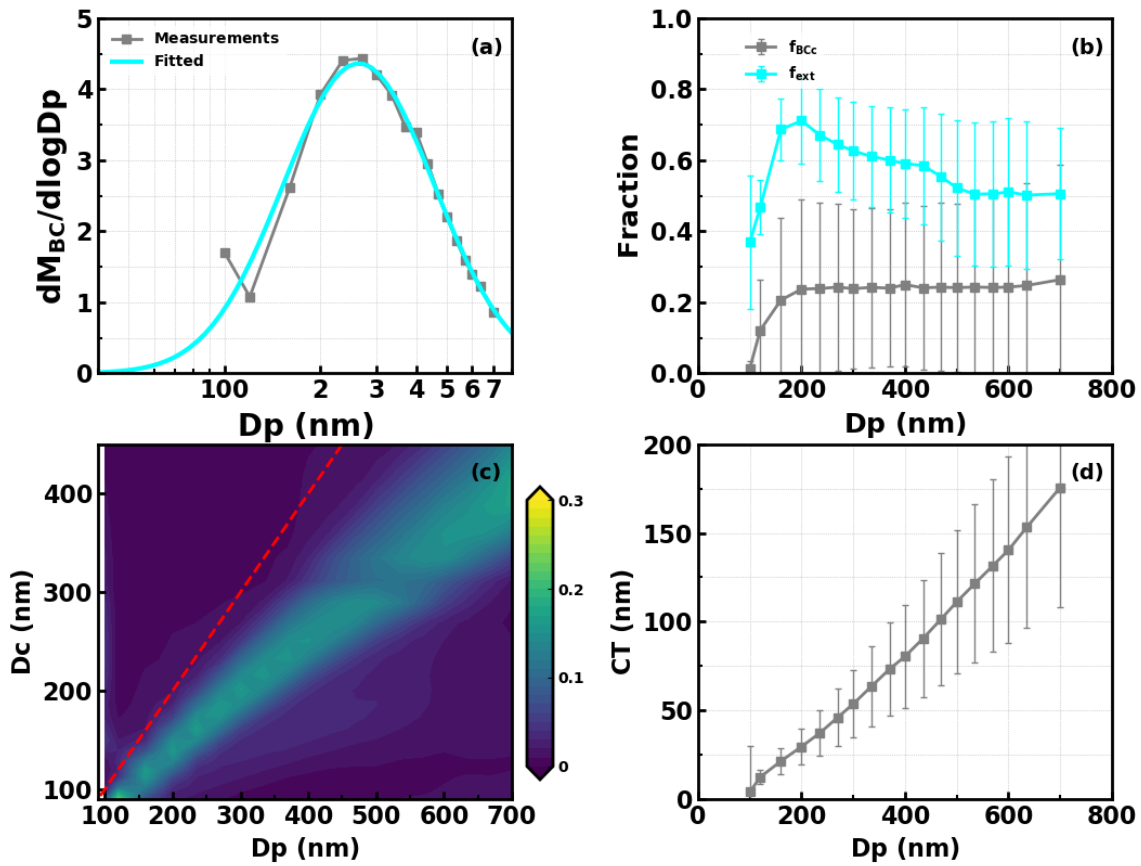
Figure 3. (a) Observed average BCMSD and the lognormal fitting curve; (b) Fractions of identified BC-containing aerosols in all aerosols at different diameters and fractions of externally mixed BC (bare BC) in BC-containing aerosols; (c) Average Dc distributions at different diameters, the red dashed line is the 1:1 line; (d) Average coating thickness (CT). Standard deviations are also shown in (b) and (d)

274 markedly different sources of rBC (Zhang et al., 2020b) and the different roles of BC-containing

275 aerosols in the formation of secondary aerosols.

276   The BC mixing state is an essential factor for determining the BC's climate effects. Fig. 3b

277 displays the average size-dependent fractions of BC-containing aerosols (f_{BCc}) and the fraction of

278   identified externally mixed (bare/thinly coated) BC particles (f_{ext}) in all BC-containing aerosols. For

279   diameters below 200 nm, not all BC-free aerosols were detected by the SP2, so the number

280   concentration of all aerosols from SMPS measurements was used to calculate f_{BCc}. The results show a

281   decrease in f_{BCc} from 200 nm to 100 nm, reaching nearly 0.01 at 100 nm. This may be due to the lower

282   fraction of BC-containing aerosols at smaller diameters, as well as the detection limit (~ 80 nm) of the

283   SP2, which may fail to detect many BC-containing aerosols below 80 nm. This can be further explained

284   based on the measurements from the volatility tandem differential mobility analyzer (V-TDMA) in

285   Guangzhou urban area in previous studies. Cheung et al. (2016) and Tan et al. (2016) used the number

286   fraction of remaining aerosols at 300 ℃ in V-TDMA measurements to represent f_{BCc}, assuming that

287   all BC-free aerosols had completely evaporated at this temperature. Their results showed an increasing

288   trend in f_{BCc} from 0.62 to 0.86 for diameters ranging from 40 nm to 300 nm, which is much higher than

289   the values reported in this study (ranging from 200 nm to 700 nm, with an average of 0.24). Both

290   methods may be biased in f_{BCc} measurements due to the detection limit of BC mass in the SP2, which

291   may underestimate f_{BCc} (Zhao et al., 2020b), and the assumption that all BC-free aerosols have

292   evaporated at 300 ℃ in V-TDMA may overestimate f_{BCc} by miscounting some aerosols with extremely

293   low volatility components (Tasoglou et al., 2020). Nevertheless, the low f_{BCc} values obtained from

294   previous V-TDMA measurements confirm that f_{BCc} is smaller for smaller diameters (Dp<200 nm). The

295   size-dependent f_{BCc} is critical for simulating aerosol optical properties (Li et al., 2019) and CCN

296   predictions (Ren et al., 2018). The facts that most BC masses reside in particles larger than 100 nm

297   and most rBC masses would be detected by SP2 suggest that the f_{BCc} reported from SP2 measurements

298   are more suitable for use in aerosol optical simulations. As for f_{ext}, the average f_{ext} shows a decreasing

299   trend from 200 nm to 700 nm, with an average of 0.59, and the f_{ext} at 100 nm being significantly

300   affected by the detection limit. This suggests that BC is generally externally mixed during the

301   observations, with a higher degree of aging for larger particles. The average distributions of rBC core

302   at different diameters are shown in Fig.3c, with a single mode at all diameters, deviating more from

303   the 1:1 line at larger diameters, again indicating a higher degree of aging for larger particles. The

304   estimated average coating thickness (CT) at different diameters is shown in Fig. 3d, with CT increasing

305   from 29 nm at 200 nm to 164 nm at 700 nm, and a relative coating thickness (RCT, Dp/Dc) ranging

306   from 1.27 at 200 nm to 1.88 at 700 nm. The RCT of 200 nm is similar to that of BC-containing aerosols

307   freshly emitted from diesel vehicles (Zhang et al., 2020b), consistent with diesel vehicle emissions

308 being the dominant source of BC traffic emissions (Bond et al., 2013).

309   The average diurnal variations of POA, rBC and secondary aerosol components including SOA,

310 AN and AS are depicted in Fig. 4a. In the morning, rBC and POA (HOA+COA) decrease due to
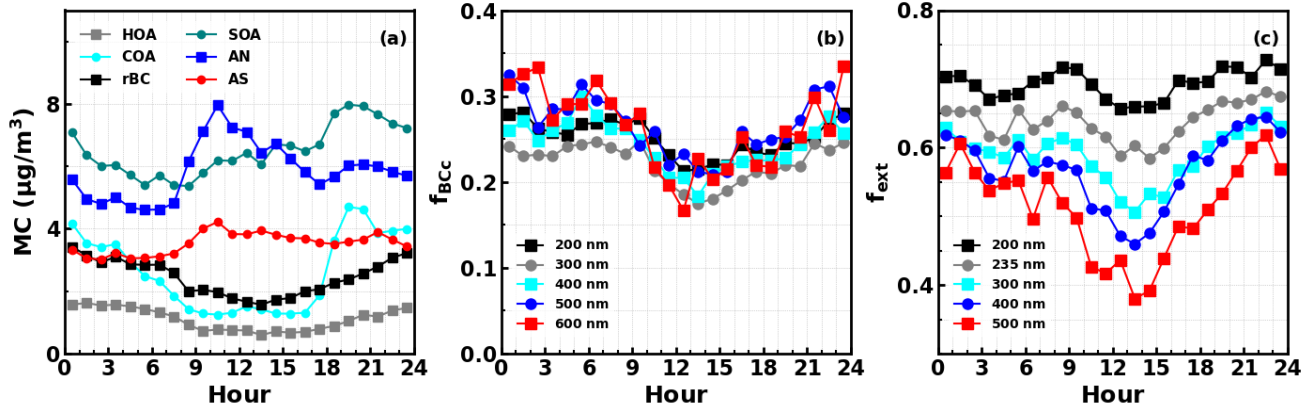
Figure 4. Average diurnal variations of **(a)** POA, SOA, ammonium nitrate (AN), ammonium sulfate (AS) and rBC ; **(b)** f_{BCc} at different diameters; **(c)** f_{ext} at different diameters.

311 dilution effects associated with boundary layer development, whereas SOA concentrations increase

312 since 08:00. However, POA and rBC begin to increase after 14:00, with the diurnal pattern of rBC

313 being generally consistent with that of HOA. The rapid increase in COA after 17:00 does not lead to a

314 significant rise in rBC, confirming that activities associated with cooking contribute negligibly to BC

315 emissions. AN and AS begin to decrease after noon, with SOA continuing to increase until 20:00,

316 which is in line with the findings reported in Zhai et al. (2022b) that the highest SOA mass

317 concentrations result from the coordination of daytime and nighttime SOA formation. The substantial

318 decrease in f_{BCc} was observed in the morning when the prominent SOA formation occur, with the

319 decrease in f_{BCc} being greater as the particle size increases, suggesting that secondary aerosols are

320 formed more efficiently on larger BC-free particles, which are then migrated to larger sizes. This is

321 further supported by the diurnal variations of f_{ext}, which revealed that secondary aerosol formation is

322 more efficient in larger BC-containing aerosols (Fig. 4c). A decrease in f_{ext} from the morning to the

323 afternoon was most prominent for aerosols at 500 nm (0.17), while a small decrease in f_{ext} (0.05) was

324 observed at 200 nm. This is consistent with the findings from the coating thickness results in Fig. 3d,

325 which showed that larger particles have higher coating thickness, and are therefore likely to contain

326 more aerosol water, thus favoring secondary aerosol formation via multiphase reactions.

327

3.3 Impacts of primary emissions and secondary aerosol formation on BC mass size distributions

The diurnal variations of f_{ext} revealed that secondary aerosols are formed on BC-containing
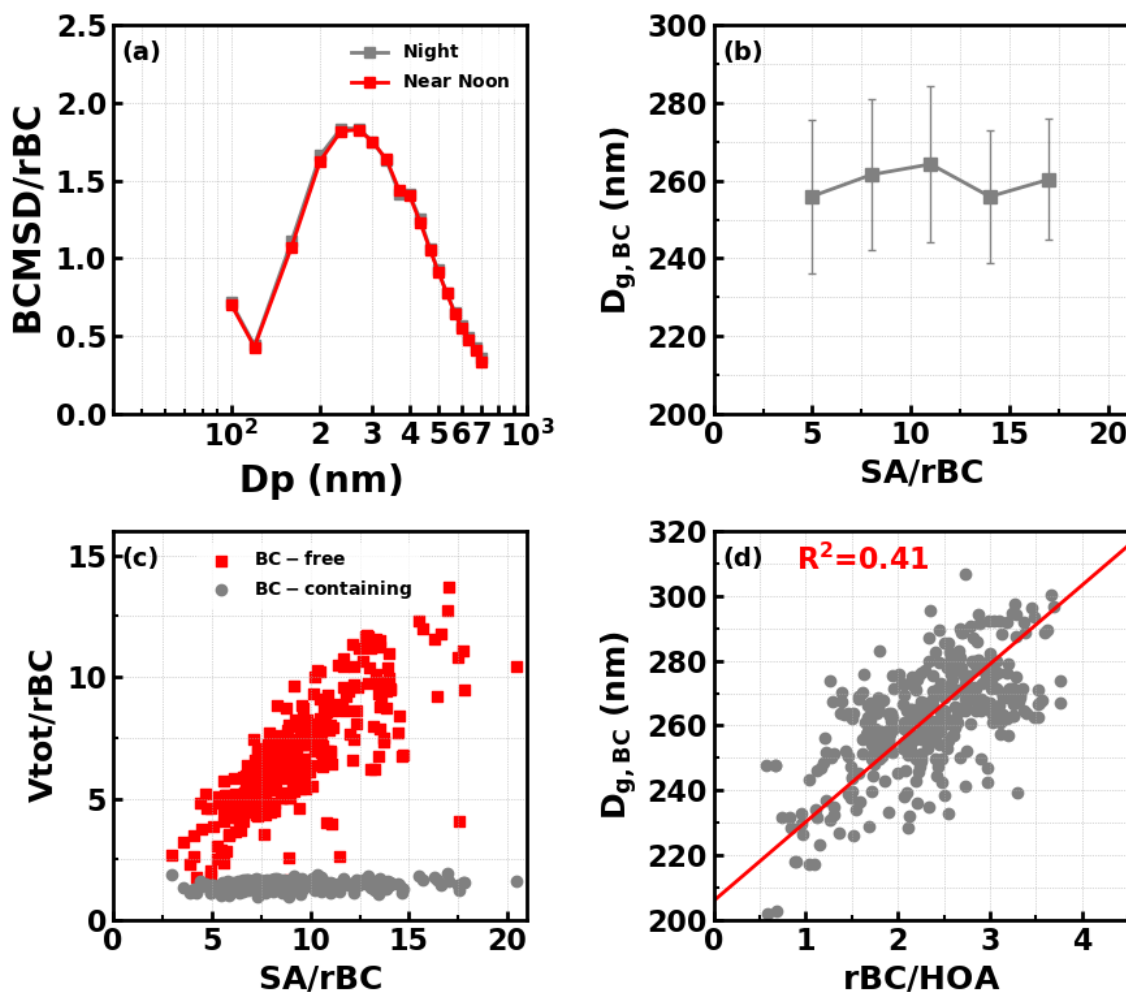
Figure 5. (a) Normalized average BCMSD during night and daytime; (b) Average variations of Dg as a function of the ratio SA/rBC, error bars are standard deviations; (c) Scatter plots of SA/rBC and the ratio total volume (Vtot) to rBC of BC free and BC containing aerosols; (d) Correlations between $D_{g,BC}$ and HOA/rBC variations during night.

aerosols, thus impacting mixing states, and this might also result in changes in BC mass size distribution. The average BC mass size distributions are shown in Fig. 5a, which are normalized with rBC during the night (from local time 20:00 to 06:00 the next morning) and during afternoon when active secondary aerosol formation is at its final stage and the impacts of accumulations of primary emissions are relatively small (local time 12:00 to 17:00). Fig.5a indicates that daytime secondary aerosol formation does not modify the shape of BC mass size distributions, which is confirmed by the variations of $D_{g,BC}$ as a function of SA/rBC ratio shown in Fig. 5b (where SA includes mass concentrations of sulfate, nitrate, ammonium and SOA). The DMA-SP2 measurements distinguish

BC-free and BC-containing aerosols, allowing for the volume variations of BC-free and BC-containing aerosols with contributions of secondary aerosol formation to be differentiated. As seen in Fig. 5c, as SA/rBC increases, the total volume of BC-containing aerosols increases very slightly, while secondary aerosol formation mainly adds mass to BC-free aerosols, explaining the same BC mass size distribution shape during both daytime and nighttime. Many previous studies have demonstrated that BC can serve as sites for heterogenous reactions (Khalizov et al., 2010) and may even promote secondary aerosol formation, thereby playing a significant role in haze formation (Zhang et al., 2020a). Results from Zhang et al. (2021) pointed out that BC promotes sulfate formation in the urban area of Guangzhou during summer. Our results indicate that BC plays a minor role in haze formation in Guangzhou during winter, which might have significant implications for haze formation mechanisms in this region.

The BC primary emissions and their subsequent aging in the air determine the observed BC mass size distributions. The aforementioned little influences of secondary aerosol formation on BC mass size distribution evolution suggest that primary emissions played a significant role in the observed variations in the BC mass size distributions. Traffic emissions dominate BC emissions during the observations as discussed before, and diesel vehicles contribute dominantly to BC emissions from traffic activities (Bond et al., 2013). The results from previous studies indicate that the ratio of elemental carbon (EC) to organic carbon (OC) changed significantly depending on the external factors (Adler et al., 2010;Lu et al., 2012), such as vehicle type, engine load, and driving conditions, etc. This ratio represents the emission conditions of diesel vehicles, which also influences the size distributions of diesel exhaust particles (Lähde et al., 2011;Han et al., 2019). Here, we use the ratio rBC/HOA to represent different emission conditions related to traffic activities and investigate the potential effects of rBC/HOA variations on BC mass size distributions. To avoid the potential effects of secondary aerosol formation and daytime evaporation of HOA due to dilution, only data points from nighttime (from 18:00 to 06:00 the next morning) are used, the results of which are displayed in Fig. 5d. Our results showed for the first time that variations of $D_{g,BC}$ are strongly correlated with rBC/HOA, and a linear relationship of $D_{g,BC}= 34 \times rBC/HOA+177$ can be derived, indicating that a larger particle diameter of BC-containing aerosols is associated with a higher BC content. Even though rBC and HOA during nighttime in this study are accumulated from different vehicle sources, the relationship between $D_{g,BC}$ and rBC/HOA still holds, suggesting that the black carbon content might be used for parametrizing BC mass size distributions in traffic-related emissions.

368

3.4 Impacts of primary emissions and secondary aerosol formation on BC mixing states

As introduced in Sect. 3.1, both f_{BCc} and f_{ext} decreased during daytime due to secondary aerosol formation. Here, the variations of daytime (from 08:00 to 18:00) f_{BCc} and f_{ext} under different SA/rBC conditions were directly investigated and shown in Fig. 6. The f_{BCc} values ranging from 200 nm to 600 nm decreased from about 0.3 to around 0.175 as SA/rBC increased from 5 to 15 (Fig. 6a), highlighting significant impacts of secondary aerosol formation on f_{BCc}. As discussed in Sect. 3.1, the decrease of f_{BCc} should be associated with the fact that secondary aerosols are formed much more quickly on BC-free aerosols than on BC-containing aerosols, which is consistent with the conclusion in Sect. 3.2 that secondary aerosol formation mainly adds mass to BC-containing aerosols. New particle formation also increases the number concentration of BC-free aerosols; however, its impact is limited for aerosol particles beyond 200 nm (Zhang et al., 2012). The evolution of particle number size distribution shape
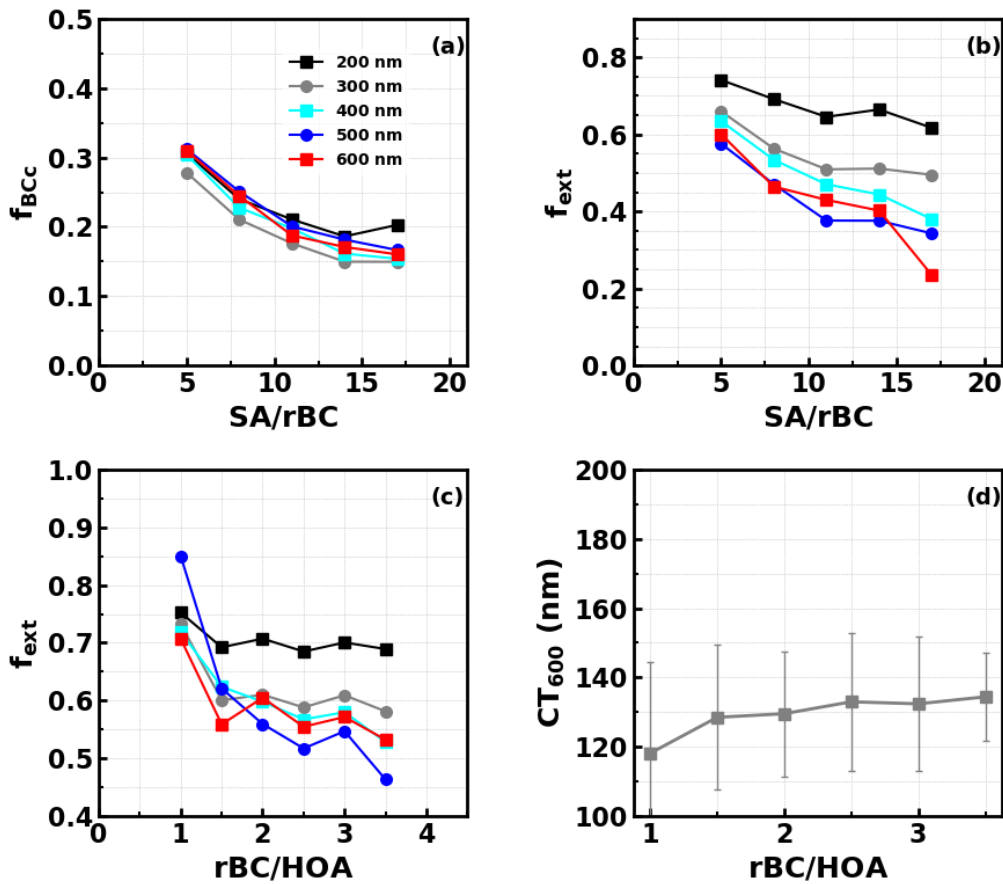
Figure 6. Variations of f_{BCc} **(a)** and **(b)** f_{ext} under different SA/rBC conditions; Variations of f_{ext} **(c)** and coating thickness of aerosols with diameter of 600 nm **(d)** under different rBC/HOA conditions, bars represent standard deviations.

beyond 200 nm is mainly associated with vapor condensation, although coagulation also play a role (Seinfeld and Pandis, 2016).

The variations in f_{ext} under different SA/rBC conditions are presented in Fig. 6b. Larger particles exhibited a more significant decrease in f_{ext} with SA/rBC increasing from 5 to 17.5, for example, f_{ext} of 200 nm particles only decreased from 0.75 to 0.6, while that of 600 nm particles decreased from 0.6 to 0.24. Aside from secondary aerosol formation, the emission conditions are also important factors that influence BC mixing states, particularly due to the contribution of the co-emitted intrinsic organic aerosols (Adler et al., 2010). At night, the shallow boundary layer facilitates the accumulation of freshly emitted aerosols, leading to increases in the mass concentrations of rBC and POA (Fig. 4a) and the mixing of freshly emitted and aged aerosols. Even so, the variations of f_{ext} during night under different rBC/HOA conditions might shed some lights on the impacts of primary emissions on BC mixing states, which is shown in Fig.6c. As rBC/HOA increased from 1 to 3.5, f_{ext} generally decreased, especially for particles larger than 300 nm. The f_{ext} of 600 nm decreased from 0.82 to 0.46, which is higher than the degree of variations influenced by secondary aerosol formation as shown in Fig. 6b, and most importantly SA/rBC decreased from 9.4 to 6.9 as rBC/HOA increased from 1 to 3.5, demonstrating that the change of emission conditions has dominated the nighttime variations of BC mixing states. The increased internal mixing degree of BC observed under higher rBC/HOA conditions is also reflected in the variations of the average coating thickness of BC-containing aerosols. As seen in Fig. 6d, the coating thickness of 600 nm BC-containing aerosols increased from 118 nm to 134 nm as rBC/HOA increased from 1 to 3.5. Interestingly, as rBC/HOA increases, the relative amount of coating to rBC becomes less, however, both fractions of internally mixed BC and coating thickness increase, suggesting that a higher fraction of co-emitted intrinsic OA resides in BC-containing aerosols. This section demonstrates the significant impacts of emission conditions of traffic sources on BC mixing states.

4. Atmospheric implications

In this study, characterizations of BC mass size distributions and mixing state and their influencing factors were first investigated using measurements of DMA-SP2 system and aerosol mass spectrometer in Guangzhou urban area. Traffic emissions are the dominant source of atmospheric BC during the observations. The lognormal distribution represents well the BC mass size distribution, with the geometric mean varying between 200 and 300 nm with an average of 258±16 nm. On one hand,

the evidence that the secondary aerosol formation mainly adds mass to BC-free particles suggests that reactions occurring on or within BC-containing particles play a limited role in the formation of haze in winter of Guangzhou. The urban area in Guangzhou is quite representative of most urban regions where traffic emissions are the primary source of BC emissions. Hence, the above finding has important implications for the haze formation mechanisms, particularly in Southern China where primary aerosol emissions and meteorological conditions are similar to those in Guangzhou. On the other hand, it was found that the daytime secondary aerosol formation reduced both f_{BCc} and f_{ext}, with the decrease of f_{ext} being more pronounced for larger particles, suggesting that secondary aerosols actually formed on BC containing aerosols though their contribution to haze formation is small. The size and mixing states of BC-containing particles determine their optical and hygroscopic properties, and are therefore critical factors for evaluating the environmental, health, and climate effects of BC; however, these factors are not adequately considered in both chemical transport and climate models (Bond et al., 2013;Saleh, 2020). The finding that secondary aerosol formation has little effect on the BC mass size distribution suggests that the study provides an excellent case scenario to investigate how changes in traffic emissions affect the BC mass size distribution and mixing states. It further shows that BC content in traffic emissions has a significant impact on both the BC mass size distribution and mixing states, and the almost linear trends between $D_{g,BC}$ and rBC/HOA suggest that BC content can be used as the key factor to parameterize both the BC mass size distribution and mixing states from traffic emissions, which warrants future comprehensive investigation.

Traffic is a major global contributor to atmospheric BC concentrations, but other major sources, such as biomass burning and coal combustion, as well as off-road diesel engines, also contribute significantly to BC emissions and play an even more important role than traffic in some regions (Bond et al., 2013). It is hence also important to investigate whether BC content of other major BC sources than traffic are important in determining BC mass size distributions and mixing states. Saleh et al. (2014) found that BC content has a major effect on the brownness of organic aerosols emitted from biomass burning, and results from several later studies further confirmed this finding (Luo et al., 2022). Recently, Saleh (2020a) discussed the potential for parameterizing the optical properties of brown carbon using BC content in climate models. Moreover, the results of Luo et al. (2022) demonstrated that BC content can also be used to parameterize the volume size distributions of aerosols emitted from biomass burning, indicating that BC content plays an important role in both traffic emissions and

biomass burning emissions. These findings suggest that more comprehensive experiments should be designed in the future to investigate the factors that control variations in BC mass size distributions and mixing states, and to discuss how to use BC content from different major BC sources for parameterizing BC mass size distributions and mixing states.

Data availability. All data needed are presented in time series of Figures and supplementary Figures, raw datasets of this study are available from the corresponding author Ye Kuang (kuangye@jnu.edu.cn) upon request.

Competing interests. The authors declare that they have no conflict of interest.

Author Contributions. YK and LL planned this campaign, with YK conceived and led this research. FL performed the data analysis and wrote the manuscript together with YK. BL made the DMA-SP2, SMPS and AE33 measurements together with FL and performed the post-processing of the SP2 data with help of GZ, MMZ maintained the Q-ACSM during the observations and performed the PMF analysis. JZ performed fund acquisition and supervision. TD, XJD and HBT helped the data acquisition and revised the manuscript. All authors reviewed and edited the manuscript.

Acknowledgments

This work is supported by the Guangdong Major Project of Basic and Applied Basic Research (Grant No. 2020B0301030004) ;Natural Science Foundation of Fujian Province (2021J01463); National Natural Science Foundation of China (42175083 and 42105092); Guangdong Provincial Key Research and Development Program (2020B1111360003); Guangdong Basic and Applied Basic Research

469 Foundation (2019A1515110791); The Special Fund Project for Science and Technology Innovation

470 Strategy of Guangdong Province (Grant No.2019B121205004).

471

472

473

References

Adler, G., Riziq, A. A., Erlick, C., and Rudich, Y.: Effect of intrinsic organic carbon on the optical properties of fresh diesel soot, Proceedings of the National Academy of Sciences, 107, 6699-6704, 10.1073/pnas.0903311106, 2010.

Bond, T. C., Habib, G., and Bergstrom, R. W.: Limitations in the enhancement of visible light absorption due to mixing state, Journal of Geophysical Research: Atmospheres, 111, https://doi.org/10.1029/2006JD007315, 2006.

Bond, T. C., Doherty, S. J., Fahey, D. W., Forster, P. M., Berntsen, T., DeAngelo, B. J., Flanner, M. G., Ghan, S., Kärcher, B., Koch, D., Kinne, S., Kondo, Y., Quinn, P. K., Sarofim, M. C., Schultz, M. G., Schulz, M., Venkataraman, C., Zhang, H., Zhang, S., Bellouin, N., Guttikunda, S. K., Hopke, P. K., Jacobson, M. Z., Kaiser, J. W., Klimont, Z., Lohmann, U., Schwarz, J. P., Shindell, D., Storelvmo, T., Warren, S. G., and Zender, C. S.: Bounding the role of black carbon in the climate system: A scientific assessment, Journal of Geophysical Research: Atmospheres, 118, 5380-5552, https://doi.org/10.1002/jgrd.50171, 2013.

Canonaco, F., Crippa, M., Slowik, J. G., Baltensperger, U., and Prévôt, A. S. H.: SoFi, an IGOR-based interface for the efficient use of the generalized multilinear engine (ME-2) for the source apportionment: ME-2 application to aerosol mass spectrometer data, Atmos. Meas. Tech., 6, 3649-3661, 10.5194/amt-6-3649-2013, 2013.

Canonaco, F., Tobler, A., Chen, G., Sosedova, Y., Slowik, J. G., Bozzetti, C., Daellenbach, K. R., El Haddad, I., Crippa, M., Huang, R. J., Furger, M., Baltensperger, U., and Prévôt, A. S. H.: A new method for long-term source apportionment with time-dependent factor profiles and uncertainty assessment using SoFi Pro: application to 1 year of organic aerosol data, Atmos. Meas. Tech., 14, 923-943, 10.5194/amt-14-923-2021, 2021.

Chen, C., Tan, H., Hong, Y., Yin, C., Deng, X., Chen, B., Wu, M., Bu, Q., Weng, J., and Gan, Q.: Characteristics, formation mechanisms, and sources of non-refractory submicron aerosols in Guangzhou, China, Atmospheric Environment, 118255, https://doi.org/10.1016/j.atmosenv.2021.118255, 2021a.

Chen, W., Ye, Y., Hu, W., Zhou, H., Pan, T., Wang, Y., Song, W., Song, Q., Ye, C., Wang, C., Wang, B., Huang, S., Yuan, B., Zhu, M., Lian, X., Zhang, G., Bi, X., Jiang, F., Liu, J., Canonaco, F., Prevot, A. S. H., Shao, M., and Wang, X.: Real-Time Characterization of Aerosol Compositions, Sources, and Aging Processes in Guangzhou During PRIDE-GBA 2018 Campaign, Journal of Geophysical Research: Atmospheres, 126, e2021JD035114, https://doi.org/10.1029/2021JD035114, 2021b.

Cheung, H. H. Y., Tan, H., Xu, H., Li, F., Wu, C., Yu, J. Z., and Chan, C. K.: Measurements of non-volatile aerosols with a VTDMA and their correlations with carbonaceous aerosols in Guangzhou, China, Atmos. Chem. Phys., 16, 8431-8446, 10.5194/acp-16-8431-2016, 2016.

Ding, A. J., Huang, X., Nie, W., Sun, J. N., Kerminen, V.-M., Petäjä, T., Su, H., Cheng, Y. F., Yang, X.-Q., Wang, M. H., Chi, X. G., Wang, J. P., Virkkula, A., Guo, W. D., Yuan, J., Wang, S. Y., Zhang, R. J., Wu, Y. F., Song, Y., Zhu, T., Zilitinkevich, S., Kulmala, M., and Fu, C. B.: Enhanced haze pollution by black carbon in megacities in China, Geophysical Research Letters, 43, 2873-2879, 10.1002/2016gl067745, 2016.

Ding, S., Liu, D., Zhao, D., Hu, K., Tian, P., Zhou, W., Huang, M., Yang, Y., Wang, F., Sheng, J., Liu, Q., Kong, S., Cui, P., Huang, Y., He, H., Coe, H., and Ding, D.: Size-Related Physical Properties of Black Carbon in the Lower Atmosphere over Beijing and Europe, Environmental science & technology, 10.1021/acs.est.9b03722, 2019.

Drinovec, L., Močnik, G., Zotter, P., Prévôt, A. S. H., Ruckstuhl, C., Coz, E., Rupakheti, M., Sciare, J., Müller, T., Wiedensohler, A., and Hansen, A. D. A.: The "dual-spot" Aethalometer: an improved measurement of aerosol black carbon with real-time loading compensation, Atmospheric Measurement Techniques, 8, 1965-1979, 10.5194/amt-8-1965-2015, 2015.

Fierce, L., Onasch, T. B., Cappa, C. D., Mazzoleni, C., China, S., Bhandari, J., Davidovits, P., Fischer, D. A., Helgestad, T., Lambe, A. T., Sedlacek, A. J., 3rd, Smith, G. D., and Wolff, L.: Radiative absorption enhancements by black carbon controlled by particle-to-particle heterogeneity in composition, Proc Natl Acad Sci U S A, 117, 5196-5203, 10.1073/pnas.1919723117, 2020.

Fröhlich, R., Cubison, M. J., Slowik, J. G., Bukowiecki, N., Prévôt, A. S. H., Baltensperger, U., Schneider, J., Kimmel, J. R.,

517   Gonin, M., Rohner, U., Worsnop, D. R., and Jayne, J. T.: The ToF-ACSM: a portable aerosol chemical speciation monitor

518   with TOFMS detection, Atmos. Meas. Tech., 6, 3225-3241, 10.5194/amt-6-3225-2013, 2013.

519   Guo, J., Zhou, S., Cai, M., Zhao, J., Song, W., Zhao, W., Hu, W., Sun, Y., He, Y., Yang, C., Xu, X., Zhang, Z., Cheng, P., Fan, Q.,

520   Hang, J., Fan, S., Wang, X., and Wang, X.: Characterization of submicron particles by time-of-flight aerosol chemical

521   speciation monitor (ToF-ACSM) during wintertime: aerosol composition, sources, and chemical processes in Guangzhou,

522   China, Atmospheric Chemistry and Physics, 20, 7595-7615, 10.5194/acp-20-7595-2020, 2020.

523   Gysel, M., Crosier, J., Topping, D. O., Whitehead, J. D., Bower, K. N., Cubison, M. J., Williams, P. I., Flynn, M. J., McFiggans,

524   G. B., and Coe, H.: Closure study between chemical composition and hygroscopic growth of aerosol particles during

525   TORCH2, Atmos. Chem. Phys., 7, 6131-6144, 10.5194/acp-7-6131-2007, 2007.

526   Han, C., Li, S.-M., Liu, P., and Lee, P.: Size Dependence of the Physical Characteristics of Particles Containing Refractory

527   Black Carbon in Diesel Vehicle Exhaust, Environmental science & technology, 53, 137-145, 10.1021/acs.est.8b04603, 2019.

528   Hu, D., Liu, D., Kong, S., Zhao, D., Wu, Y., Li, S., Ding, S., Zheng, S., Cheng, Y., Hu, K., Deng, Z., Wu, Y., Tian, P., Liu, Q., Huang,

529   M., and Ding, D.: Direct Quantification of Droplet Activation of Ambient Black Carbon Under Water Supersaturation,

530   Journal of Geophysical Research: Atmospheres, 126, e2021JD034649, https://doi.org/10.1029/2021JD034649, 2021.

531   Hu, M., Peng, J., Sun, K., Yue, D., Guo, S., Wiedensohler, A., and Wu, Z.: Estimation of Size-Resolved Ambient Particle

532   Density Based on the Measurement of Aerosol Number, Mass, and Chemical Size Distributions in the Winter in Beijing,

533   Environmental science & technology, 46, 9941-9947, 10.1021/es204073t, 2012.

534   Khalizov, A. F., Cruz-Quinones, M., and Zhang, R.: Heterogeneous Reaction of NO2 on Fresh and Coated Soot Surfaces, The

535   Journal of Physical Chemistry A, 114, 7516-7524, 10.1021/jp1021938, 2010.

536   Koch, D., and Del Genio, A. D.: Black carbon semi-direct effects on cloud cover: review and synthesis, Atmos. Chem. Phys.,

537   10, 7685-7696, 10.5194/acp-10-7685-2010, 2010.

538   Kompalli, S. K., Suresh Babu, S. N., Satheesh, S. K., Krishna Moorthy, K., Das, T., Boopathy, R., Liu, D., Darbyshire, E., Allan,

539   J. D., Brooks, J., Flynn, M. J., and Coe, H.: Seasonal contrast in size distributions and mixing state of black carbon and its

540   association with PM1.0 chemical composition from the eastern coast of India, Atmos. Chem. Phys., 20, 3965-3985,

541   10.5194/acp-20-3965-2020, 2020.

542   Kuang, Y., He, Y., Xu, W., Yuan, B., Zhang, G., Ma, Z., Wu, C., Wang, C., Wang, S., Zhang, S., Tao, J., Ma, N., Su, H., Cheng, Y.,

543   Shao, M., and Sun, Y.: Photochemical Aqueous-Phase Reactions Induce Rapid Daytime Formation of Oxygenated Organic

544   Aerosol on the North China Plain, Environmental science & technology, 54, 3849-3860, 10.1021/acs.est.9b06836, 2020.

545   Lähde, T., Rönkkö, T., Happonen, M., Söderström, C., Virtanen, A., Solla, A., Kytö, M., Rothe, D., and Keskinen, J.: Effect of

546   Fuel Injection Pressure on a Heavy-Duty Diesel Engine Nonvolatile Particle Emission, Environmental science & technology,

547   45, 2504-2509, 10.1021/es103431p, 2011.

548   Li, Z., Tan, H., Zheng, J., Liu, L., Qin, Y., Wang, N., Li, F., Li, Y., Cai, M., Ma, Y., and Chan, C. K.: Light absorption properties

549   and potential sources of particulate brown carbon in the Pearl River Delta region of China, Atmos. Chem. Phys., 19, 11669-

550   11685, 10.5194/acp-19-11669-2019, 2019.

551   Liu, D., Allan, J., Whitehead, J., Young, D., Flynn, M., Coe, H., McFiggans, G., Fleming, Z. L., and Bandy, B.: Ambient black

552   carbon particle hygroscopic properties controlled by mixing state and composition, Atmospheric Chemistry and Physics,

553   13, 2015-2029, 10.5194/acp-13-2015-2013, 2013.

554   Liu, D., Whitehead, J., Alfarra, M. R., Reyes-Villegas, E., Spracklen, D. V., Reddington, C. L., Kong, S., Williams, P. I., Ting, Y.-

555   C., Haslett, S., Taylor, J. W., Flynn, M. J., Morgan, W. T., McFiggans, G., Coe, H., and Allan, J. D.: Black-carbon absorption

556   enhancement in the atmosphere determined by particle mixing state, Nature Geosci, advance online publication,

557   10.1038/ngeo2901

558   http://www.nature.com/ngeo/journal/vaop/ncurrent/abs/ngeo2901.html#supplementary-information, 2017.

559   Liu, D., Joshi, R., Wang, J., Yu, C., Allan, J. D., Coe, H., Flynn, M. J., Xie, C., Lee, J., Squires, F., Kotthaus, S., Grimmond, S.,

560   Ge, X., Sun, Y., and Fu, P.: Contrasting physical properties of black carbon in urban Beijing between winter and summer,

Atmos. Chem. Phys., 19, 6749-6769, 10.5194/acp-19-6749-2019, 2019.

Liu, J., Li, J., Zhang, Y., Liu, D., Ding, P., Shen, C., Shen, K., He, Q., Ding, X., Wang, X., Chen, D., Szidat, S., and Zhang, G.: Source apportionment using radiocarbon and organic tracers for PM2.5 carbonaceous aerosols in Guangzhou, South China: contrasting local- and regional-scale haze events, Environmental science & technology, 48, 12002-12011, 10.1021/es503102w, 2014.

Liu, L., Kuang, Y., Zhai, M., Xue, B., He, Y., Tao, J., Luo, B., Xu, W., Tao, J., Yin, C., Li, F., Xu, H., Deng, T., Deng, X., Tan, H., and Shao, M.: Strong light scattering of highly oxygenated organic aerosols impacts significantly on visibility degradation, Atmos. Chem. Phys., 22, 7713-7726, 10.5194/acp-22-7713-2022, 2022.

Lu, T., Cheung, C. S., and Huang, Z.: Size-Resolved Volatility, Morphology, Nanostructure, and Oxidation Characteristics of Diesel Particulate, Energy & Fuels, 26, 6168-6176, 10.1021/ef3010527, 2012.

Luo, B., Kuang, Y., Huang, S., Song, Q., Hu, W., Li, W., Peng, Y., Chen, D., Yue, D., Yuan, B., and Shao, M.: Parameterizations of size distribution and refractive index of biomass burning organic aerosol with black carbon content, Atmos. Chem. Phys., 22, 12401-12415, 10.5194/acp-22-12401-2022, 2022.

Man, R., Wu, Z., Zong, T., Voliotis, A., Qiu, Y., Größ, J., van Pinxteren, D., Zeng, L., Herrmann, H., Wiedensohler, A., and Hu, M.: Impact of water uptake and mixing state on submicron particle deposition in the human respiratory tract (HRT) based on explicit hygroscopicity measurements at HRT-like conditions, Atmos. Chem. Phys., 22, 12387-12399, 10.5194/acp-22-12387-2022, 2022.

Menon, S., Hansen, J., Nazarenko, L., and Luo, Y.: Climate Effects of Black Carbon Aerosols in China and India, Science, 297, 2250-2253, doi:10.1126/science.1075159, 2002.

Middlebrook, A. M., Bahreini, R., Jimenez, J. L., and Canagaratna, M. R.: Evaluation of Composition-Dependent Collection Efficiencies for the Aerodyne Aerosol Mass Spectrometer using Field Data, Aerosol Science and Technology, 46, 258-271, 10.1080/02786826.2011.620041, 2012.

Moteki, N., and Kondo, Y.: Effects of Mixing State on Black Carbon Measurements by Laser-Induced Incandescence, Aerosol Science and Technology, 41, 398-417, 10.1080/02786820701199728, 2007.

Motos, G., Schmale, J., Corbin, J. C., Modini, R. L., Karlen, N., Bertò, M., Baltensperger, U., and Gysel-Beer, M.: Cloud droplet activation properties and scavenged fraction of black carbon in liquid-phase clouds at the high-alpine research station Jungfraujoch (3580 m a.s.l.), Atmos. Chem. Phys., 19, 3833-3855, 10.5194/acp-19-3833-2019, 2019.

Ng, N. L., Herndon, S. C., Trimborn, A., Canagaratna, M. R., Croteau, P. L., Onasch, T. B., Sueper, D., Worsnop, D. R., Zhang, Q., Sun, Y. L., and Jayne, J. T.: An Aerosol Chemical Speciation Monitor (ACSM) for Routine Monitoring of the Composition and Mass Concentrations of Ambient Aerosol, Aerosol Science and Technology, 45, 780-794, Pii 934555189 10.1080/02786826.2011.560211, 2011.

Nichols, J. L., Owens, E. O., Dutton, S. J., and Luben, T. J.: Systematic review of the effects of black carbon on cardiovascular disease among individuals with pre-existing disease, International Journal of Public Health, 58, 707-724, 10.1007/s00038-013-0492-z, 2013.

Ning, Z., Chan, K. L., Wong, K. C., Westerdahl, D., Močnik, G., Zhou, J. H., and Cheung, C. S.: Black carbon mass size distributions of diesel exhaust and urban aerosols measured using differential mobility analyzer in tandem with Aethalometer, Atmospheric Environment, 80, 31-40, https://doi.org/10.1016/j.atmosenv.2013.07.037, 2013.

Peng, J., Hu, M., Guo, S., Du, Z., Zheng, J., Shang, D., Levy Zamora, M., Zeng, L., Shao, M., Wu, Y.-S., Zheng, J., Wang, Y., Glen, C. R., Collins, D. R., Molina, M. J., and Zhang, R.: Markedly enhanced absorption and direct radiative forcing of black carbon under polluted urban environments, Proceedings of the National Academy of Sciences, 10.1073/pnas.1602310113, 2016.

Raatikainen, T., Brus, D., Hooda, R. K., Hyvärinen, A. P., Asmi, E., Sharma, V. P., Arola, A., and Lihavainen, H.: Size-selected black carbon mass distributions and mixing state in polluted and clean environments of northern India, Atmos. Chem.

605 Phys., 17, 371-383, 10.5194/acp-17-371-2017, 2017.

606 Ren, J., Zhang, F., Wang, Y., Collins, D., Fan, X., Jin, X., Xu, W., Sun, Y., Cribb, M., and Li, Z.: Using different assumptions of
607 aerosol mixing state and chemical composition to predict CCN concentrations based on field measurements in urban
608 Beijing, Atmos. Chem. Phys., 18, 6907-6921, 10.5194/acp-18-6907-2018, 2018.

609 Saleh, R., Robinson, E. S., Tkacik, D. S., Ahern, A. T., Liu, S., Aiken, A. C., Sullivan, R. C., Presto, A. A., Dubey, M. K., Yokelson,
610 R. J., Donahue, N. M., and Robinson, A. L.: Brownness of organics in aerosols from biomass burning linked to their black
611 carbon content, Nature Geoscience, 7, 647, 10.1038/ngeo2220
612 https://www.nature.com/articles/ngeo2220#supplementary-information, 2014.

613 Saleh, R.: From Measurements to Models: Toward Accurate Representation of Brown Carbon in Climate Calculations,
614 Current Pollution Reports, 10.1007/s40726-020-00139-3, 2020.

615 Sarangi, B., Ramachandran, S., Rajesh, T. A., and Dhaker, V. K.: Characteristics of black carbon aerosol mixing state over an
616 urban region deduced using single particle soot photometer (SP2) and differential mobility analyzer (DMA), Atmospheric
617 Pollution Research, 11, 574-582, https://doi.org/10.1016/j.apr.2019.12.006, 2020.

618 Schwarz, J. P., Gao, R. S., Fahey, D. W., Thomson, D. S., Watts, L. A., Wilson, J. C., Reeves, J. M., Darbeheshti, M.,
619 Baumgardner, D. G., Kok, G. L., Chung, S. H., Schulz, M., Hendricks, J., Lauer, A., Kärcher, B., Slowik, J. G., Rosenlof, K. H.,
620 Thompson, T. L., Langford, A. O., Loewenstein, M., and Aikin, K. C.: Single-particle measurements of midlatitude black
621 carbon and light-scattering aerosols from the boundary layer to the lower stratosphere, Journal of Geophysical Research:
622 Atmospheres, 111, D16207, 10.1029/2006JD007076, 2006.

623 Sedlacek Iii, A. J., Lewis, E. R., Kleinman, L., Xu, J., and Zhang, Q.: Determination of and evidence for non-core-shell
624 structure of particles containing black carbon using the Single-Particle Soot Photometer (SP2), Geophysical Research
625 Letters, 39, https://doi.org/10.1029/2012GL050905, 2012.

626 Seinfeld, J., and Pandis, S.: Atmospheric Chemistry and Physics: From Air Pollution to Climate Change, Third Edition, 2016.

627 Stabile, L., Fuoco, F. C., and Buonanno, G.: Characteristics of particles and black carbon emitted by combustion of incenses,
628 candles and anti-mosquito products, Building and Environment, 56, 184-191,
629 https://doi.org/10.1016/j.buildenv.2012.03.005, 2012.

630 Sun, J. Y., Wu, C., Wu, D., Cheng, C., Li, M., Li, L., Deng, T., Yu, J. Z., Li, Y. J., Zhou, Q., Liang, Y., Sun, T., Song, L., Cheng, P.,
631 Yang, W., Pei, C., Chen, Y., Cen, Y., Nian, H., and Zhou, Z.: Amplification of black carbon light absorption induced by
632 atmospheric aging: temporal variation at seasonal and diel scales in urban Guangzhou, Atmospheric Chemistry and
633 Physics, 20, 2445-2470, 10.5194/acp-20-2445-2020, 2020.

634 Tan, H., Liu, L., Fan, S., Li, F., Yin, Y., Cai, M., and Chan, P. W.: Aerosol optical properties and mixing state of black carbon in
635 the Pearl River Delta, China, Atmospheric Environment, 131, 196-208, https://doi.org/10.1016/j.atmosenv.2016.02.003,
636 2016.

637 Tasoglou, A., Louvaris, E., Florou, K., Liangou, A., Karnezi, E., Kaltsonoudis, C., Wang, N., and Pandis, S. N.: Aerosol light
638 absorption and the role of extremely low volatility organic compounds, Atmospheric Chemistry and Physics, 20, 11625-
639 11637, 10.5194/acp-20-11625-2020, 2020.

640 Wang, Y., Khalizov, A., Levy, M., and Zhang, R.: New Directions: Light absorbing aerosols and their atmospheric impacts,
641 Atmospheric Environment, 81, 713-715, https://doi.org/10.1016/j.atmosenv.2013.09.034, 2013.

642 Wang, Y., Ma, P.-L., Peng, J., Zhang, R., Jiang, J. H., Easter, R. C., and Yung, Y. L.: Constraining Aging Processes of Black
643 Carbon in the Community Atmosphere Model Using Environmental Chamber Measurements, Journal of Advances in
644 Modeling Earth Systems, 10, 2514-2526, https://doi.org/10.1029/2018MS001387, 2018.

645 Wang, Y., Li, W., Huang, J., Liu, L., Pang, Y., He, C., Liu, F., Liu, D., Bi, L., Zhang, X., and Shi, Z.: Nonlinear Enhancement of
646 Radiative Absorption by Black Carbon in Response to Particle Mixing Structure, Geophysical Research Letters, 48,
647 e2021GL096437, https://doi.org/10.1029/2021GL096437, 2021.

648 Wiedensohler, A., Birmili, W., Nowak, A., Sonntag, A., Weinhold, K., Merkel, M., Wehner, B., Tuch, T., Pfeifer, S., Fiebig, M.,

Fjäraa, A. M., Asmi, E., Sellegri, K., Depuy, R., Venzac, H., Villani, P., Laj, P., Aalto, P., Ogren, J. A., Swietlicki, E., Williams, P., Roldin, P., Quincey, P., Hüglin, C., Fierz-Schmidhauser, R., Gysel, M., Weingartner, E., Riccobono, F., Santos, S., Grüning, C., Faloon, K., Beddows, D., Harrison, R., Monahan, C., Jennings, S. G., O'Dowd, C. D., Marinoni, A., Horn, H. G., Keck, L., Jiang, J., Scheckman, J., McMurry, P. H., Deng, Z., Zhao, C. S., Moerman, M., Henzing, B., de Leeuw, G., Löschau, G., and Bastian, S.: Mobility particle size spectrometers: harmonization of technical standards and data structure to facilitate high quality long-term observations of atmospheric particle number size distributions, Atmos. Meas. Tech., 5, 657-685, 10.5194/amt-5-657-2012, 2012.

Wilcox, E. M., Thomas, R. M., Praveen, P. S., Pistone, K., Bender, F. A.-M., and Ramanathan, V.: Black carbon solar absorption suppresses turbulence in the atmospheric boundary layer, Proceedings of the National Academy of Sciences, 113, 11794-11799, doi:10.1073/pnas.1525746113, 2016.

Wu, Y., Xia, Y., Huang, R., Deng, Z., Tian, P., Xia, X., and Zhang, R.: A study of the morphology and effective density of externally mixed black carbon aerosols in ambient air using a size-resolved single-particle soot photometer (SP2), Atmos. Meas. Tech., 12, 4347-4359, 10.5194/amt-12-4347-2019, 2019.

Xu, Z., Li, X., Guan, C., and Huang, Z.: Effects of injection timing on exhaust particle size and nanostructure on a diesel engine at different loads, Journal of Aerosol Science, 76, 28-38, https://doi.org/10.1016/j.jaerosci.2014.05.002, 2014.

Yu, C., Liu, D., Hu, K., Tian, P., Wu, Y., Zhao, D., Wu, H., Hu, D., Guo, W., Li, Q., Huang, M., Ding, D., and Allan, J. D.: Aerodynamic size-resolved composition and cloud condensation nuclei properties of aerosols in a Beijing suburban region, Atmos. Chem. Phys., 22, 4375-4391, 10.5194/acp-22-4375-2022, 2022.

Zhai, J., Yang, X., Li, L., Bai, B., Liu, P., Huang, Y., Fu, T.-M., Zhu, L., Zeng, Z., Tao, S., Lu, X., Ye, X., Wang, X., Wang, L., and Chen, J.: Absorption Enhancement of Black Carbon Aerosols Constrained by Mixing-State Heterogeneity, Environmental science & technology, 56, 1586-1593, 10.1021/acs.est.1c06180, 2022a.

Zhai, M., Kuang, Y., Liu, L., He, Y., Luo, B., Xu, W., Tao, J., Zou, Y., Li, F., Yin, C., Li, C., Xu, H., and Deng, X.: Insights into characteristics and formation mechanisms of secondary organic aerosols in Guangzhou urban area, Atmos. Chem. Phys. Discuss., 2022, 1-29, 10.5194/acp-2022-807, 2022b.

Zhang, F., Wang, Y., Peng, J., Chen, L., Sun, Y., Duan, L., Ge, X., Li, Y., Zhao, J., Liu, C., Zhang, X., Zhang, G., Pan, Y., Wang, Y., Zhang, A. L., Ji, Y., Wang, G., Hu, M., Molina, M. J., and Zhang, R.: An unexpected catalyst dominates formation and radiative forcing of regional haze, Proceedings of the National Academy of Sciences, 201919343, 10.1073/pnas.1919343117, 2020a.

Zhang, G., Lin, Q., Peng, L., Bi, X., Chen, D., Li, M., Li, L., Brechtel, F. J., Chen, J., Yan, W., Wang, X., Peng, P., amp, apos, an, Sheng, G., and Zhou, Z.: The single-particle mixing state and cloud scavenging of black carbon: a case study at a high-altitude mountain site in southern China, Atmospheric Chemistry and Physics, 17, 14975-14985, 10.5194/acp-17-14975-2017, 2017.

Zhang, G., Fu, Y., Peng, X., Sun, W., Shi, Z., Song, W., Hu, W., Chen, D., Lian, X., Li, L., Tang, M., Wang, X., and Bi, X.: Black Carbon Involved Photochemistry Enhances the Formation of Sulfate in the Ambient Atmosphere: Evidence From In Situ Individual Particle Investigation, Journal of Geophysical Research: Atmospheres, 126, e2021JD035226, https://doi.org/10.1029/2021JD035226, 2021.

Zhang, R., Khalizov, A., Wang, L., Hu, M., and Xu, W.: Nucleation and growth of nanoparticles in the atmosphere, Chem Rev, 112, 1957-2011, 10.1021/cr2001756, 2012.

Zhang, Y., Zhang, Q., Cheng, Y., Su, H., Kecorius, S., Wang, Z., Wu, Z., Hu, M., Zhu, T., Wiedensohler, A., and He, K.: Measuring the morphology and density of internally mixed black carbon with SP2 and VTDMA: new insight into the absorption enhancement of black carbon in the atmosphere, Atmospheric Measurement Techniques, 9, 1833-1843, 10.5194/amt-9-1833-2016, 2016.

Zhang, Y., Favez, O., Canonaco, F., Liu, D., Močnik, G., Amodeo, T., Sciare, J., Prévôt, A. S. H., Gros, V., and Albinet, A.: Evidence of major secondary organic aerosol contribution to lensing effect black carbon absorption enhancement, npj

693   Climate and Atmospheric Science, 1, 47, 10.1038/s41612-018-0056-2, 2018a.

694   Zhang, Y., Su, H., Ma, N., Li, G., Kecorius, S., Wang, Z., Hu, M., Zhu, T., He, K., Wiedensohler, A., Zhang, Q., and Cheng, Y.:

695   Sizing of Ambient Particles From a Single-Particle Soot Photometer Measurement to Retrieve Mixing State of Black Carbon

696   at a Regional Site of the North China Plain, Journal of Geophysical Research: Atmospheres, 123, 12,778-712,795,

697   https://doi.org/10.1029/2018JD028810, 2018b.

698   Zhang, Y., Li, Y., Guo, J., Wang, Y., Chen, D., and Chen, H.: The climatology and trend of black carbon in China from 12-year

699   ground observations, Climate Dynamics, 53, 5881-5892, 10.1007/s00382-019-04903-0, 2019.

700   Zhang, Y., Zhang, Q., Yao, Z., and Li, H.: Particle Size and Mixing State of Freshly Emitted Black Carbon from Different

701   Combustion Sources in China, Environmental science & technology, 54, 7766-7774, 10.1021/acs.est.9b07373, 2020b.

702   Zhao, G., Tao, J., Kuang, Y., Shen, C., Yu, Y., and Zhao, C.: Role of black carbon mass size distribution in the direct aerosol

703   radiative forcing, Atmos. Chem. Phys., 19, 13175-13188, 10.5194/acp-19-13175-2019, 2019.

704   Zhao, G., Li, F., and Zhao, C.: Determination of the refractive index of ambient aerosols, Atmospheric Environment, 240,

705   117800, https://doi.org/10.1016/j.atmosenv.2020.117800, 2020a.

706   Zhao, G., Shen, C., and Zhao, C.: Technical note: Mismeasurement of the core-shell structure of black carbon-containing

707   ambient aerosols by SP2 measurements, Atmospheric Environment, 243, 117885,

708   https://doi.org/10.1016/j.atmosenv.2020.117885, 2020b.

709   Zhao, G., Tan, T., Zhu, Y., Hu, M., and Zhao, C.: Method to quantify black carbon aerosol light absorption enhancement

710   with a mixing state index, Atmos. Chem. Phys., 21, 18055-18063, 10.5194/acp-21-18055-2021, 2021.

711